

IN-DEPTH *CHANDRA* STUDY OF THE AGN FEEDBACK IN VIRGO ELLIPTICAL GALAXY M84

A. FINOGENOV^{1,2}, M. RUSZKOWSKI^{3,6}, C. JONES⁴, M. BRÜGGEN⁵, A. VIKHLININ⁴, E. MANDEL⁴

ApJ in press, November 1, 2008, v687n1

ABSTRACT

Using deep *Chandra* observations of M84 we study the energetics of the interaction between the black hole and the interstellar medium of this early-type galaxy. We perform a detailed two dimensional reconstruction of the properties of the X-ray emitting gas using a constrained Voronoi tessellation method, identifying the mean trends and carrying out the fluctuation analysis of the thermodynamical properties of the hot ISM. In addition to the *PV* work associated with the bubble expansion, we identify and measure the wave energy associated with the mildly supersonic bubble expansion. We show that, depending on the age of the cavity and the associated wave, the waves can have a substantial contribution to the total energy release from the AGN. The energy dissipated in the waves tends to be concentrated near the center of M84 and in the direction perpendicular to the bubble outflow, possibly due to the interference of the waves generated by the expansion of northern and southern bubbles. We also find direct evidence for the escape of radio plasma from the ISM of the host galaxy into the intergalactic medium.

Subject headings: AGN – galaxies: intergalactic medium – galaxies: elliptical – X-rays: galaxies

1. INTRODUCTION

The detailed investigations of the balance between the heating and cooling of the hot interstellar medium (ISM) and intracluster medium (ICM) have been made possible due to the key observations made by *Chandra* and XMM-*Newton* and the successes in numerical modeling (see McNamara & Nulsen 2007 for a review). The commonly accepted paradigm states that the feedback mechanism is ultimately linked to the activity of the supermassive black holes located at the bottom of the potential wells in systems with cool cores.

A standard way of estimating the energy released by the AGN is to measure the *PV* work associated with X-ray cavities (bubbles) inflated by the AGN. This is an indirect measurement as the bubbles are typically “observed” as depressions in X-ray emissivity. However, the task of estimating the AGN energy injected into the ICM can be accomplished by assuming that such X-ray cavities are in pressure balance with the ICM. One can then infer the total energy contained in the cavities that is available for doing mechanical work (i.e., enthalpy) from $H = \gamma/(\gamma - 1)PV$, where γ is the adiabatic index, P is the pressure and V is the bubble volume. Such an observational estimate is further complicated by the fact that the effective adiabatic index γ of the material inside the bubbles is not known. That is, it is not known if the bubbles are predominantly thermal, in which case $\gamma = 5/3$ (e.g., Mazzotta et al. 2002 shows that both the thermal and non-thermal models fit the data in the case of MKW

3s galaxy cluster) or non-thermal, in which case $\gamma = 4/3$ (e.g., Sanders & Fabian 2007 in the case of the Perseus cluster). The content of radio lobes and X-ray cavities may depend on such factors as the initial jet composition ($e^+ - e^-$ or $p - e^-$), the efficacy of entrainment of colder thermal ICM gas or the magnetic pressure support inside the bubbles (Dunn et al. 2006 and references therein). Furthermore, the energy content obtained this way may be a lower limit to the actual total energy released by the AGN if the pressure balance assumption does not hold. An extreme example of this effect is seen in the simulations of very high Mach number jets interacting with the ICM (Binney, Bibi & Omma 2007).

Moreover, X-ray observations show that the standard method of inferring AGN energies leads to the bubble energy *increasing* in the statistical sense with the distance from the center of the gravitational potential (Diehl et al. 2008). This apparently counter intuitive result may be the result of the erroneous assumption that the bubbles are “born” in pressure equilibrium with the surrounding ICM or ISM.

If the bubbles are overpressured with respect to the ISM, then one would need the internal bubble pressure to correctly estimate the energy inside the bubble. Moreover, if they were overpressured in the past, then this overpressure should have created waves that have carried some portion of the energy away from the cavities. The standard method of estimating the AGN energy based on the pressure balance and cavity size does not include such contributions to the total energy balance. In addition to increasing the overall energy budget, such waves provide a more gentle and spatially-distributed heating.

The above effects clearly demonstrate the need for alternative or supplementary measurements of the energy injected by the AGN. In this Paper we report on the long time exposure observation of the elliptical galaxy M84 in the Virgo cluster. We focus on the interaction of the AGN with the ISM and the energy content in the thermodynamical fluctuations generated by the the AGN

¹ Max-Planck-Institut für Extraterrestrische Physik, Giessenbachstraße, 85748 Garching, Germany

² University of Maryland, Baltimore County, 1000 Hilltop Circle, Baltimore, MD 21250, USA

³ Department of Astronomy, University of Michigan, 500 Church Street, Ann Arbor, MI 48109-1042, USA

⁴ Harvard-Smithsonian Center for Astrophysics, 60 Garden Street, Cambridge, MA 02138, USA

⁵ Jacobs University Bremen, Campus Ring 1, 28759 Bremen, Germany

⁶ Max-Planck-Institut für Astrophysik, D-85748 Garching, Germany

outburst and argue that they are waves. An approach to measure the wave energy that is similar to the one described in this Paper, has been considered by Sanders & Fabian (2007) in the case of the observations of the Perseus cluster and in the numerical simulations of wave dissipation (Ruszkowski et al. 2004).

2. CHANDRA OBSERVATIONS

Results from the first Chandra observation of M84 (OBS ID 803 and exposure time of 25.9 ksec) were published in Finoguenov & Jones (2001, 2002). Given the importance of the source in understanding the AGN feedback, we were granted two more observations (OBS IDs 5908 and 6131) adding 34.9 and 30.9 ksec time, respectively. The nominal aim point was ACIS-S and we only include S3 CCD data here. The initial data reduction is standard and its details are presented in Vikhlinin et al. (2005).

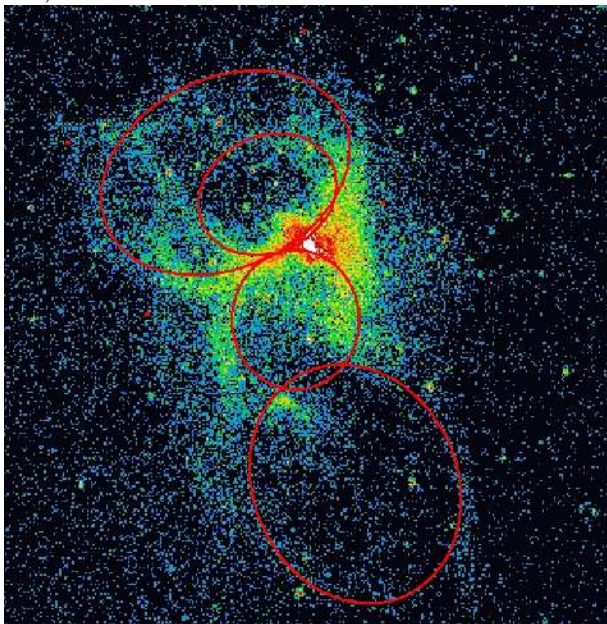


FIG. 1.— Image of M84 in the 0.5–2 keV band. Red circles show the position and size of the four identified bubbles. The image is 2.8 arcminute or 14 kpc wide on a side.

For both imaging and spectroscopic analysis we extracted the counts and the auxiliary information separately from each observation, and added it together at a final stage proportional to the exposure time. The distant-dependent parameters of the emission have been calculated assuming a 17 Mpc distance to M84 at which 1 arcminute corresponds to 5.0 kpc.

2.1. Imaging

The raw cumulative photon count ACIS-S image of M84 in the energy band 0.5–2 keV is shown in Fig.1. In addition to previously identified cavities associated with the radio bubbles, we clearly see structure in the bubbles, which can be approximated by two sets of two bubbles to the north and south of the M84 center. In Fig.2 we compare the X-ray and radio properties of M84. It is clearly seen that while the southern radio bubble is surrounded by the X-ray cocoon, the northern radio bubble broke through the porous X-ray emission at the northern edge. This provides direct evidence of escaping

radio plasma from the ISM of the host galaxy into the intergalactic medium.

This paper describes the parameters of these bubbles, with a summary of the results given in Table 1, listing name of the bubble (col. 1), position of the bubble centroid (2-3), bubble axes (major, minor, assumed projected) in kpc (4-6), effective thickness of bubble walls (7), total geometrical factor from Eq.2 (8), estimated Mach number from the pressure jump (9), PV work (enthalpy H is higher by up to a factor of 4, as explained above) (10), wave energy, calculated using Eq.2 with $\gamma = 5/3$ (11; see below). In calculating the values of columns 10 and 11 we used a 3-d integral over the bubbles and the non-parametric fit to the pressure profile of all zones of M84, as explained in §3. In calculation we use the exact pressure prediction at each dV element assuming a spherical symmetry in the pressure.

Imaging analysis provides information on the bubble appearance, such as centering, size and orientation, which enter the volume and surface calculations. The width of the bubble walls is calculated as the ratio between the distances from the bubble center to the outer and the inner boundaries, which is used in the calculation of the wave energetics; and helps to select the regions for subsequent spectral analysis, which we describe next.

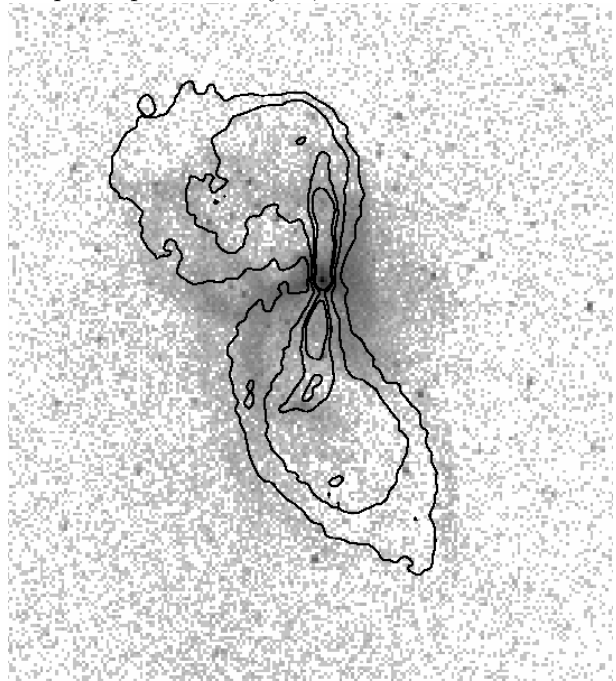


FIG. 2.— Binned raw X-ray image of M84 with radio contours overlaid. For the southern part of M84, radio emission is clearly embedded in the X-rays, while in the north it breaks through the bubbles. The image is 3.6 arcminute or 18 kpc wide on a side.

Statistics, achieved in the combined *Chandra* observation of M84, requires substantial binning of the data for the subsequent spectral analysis. The binning techniques based on the Voronoi tessellation methods have been proven to be the most efficient and unbiased way to address the binning issue (e.g. Cappellari & Copin 2003). However, in order to study the waves and bubbles, we need to separate the bubble rims from both the inner and outer medium. To accomplish this task, we produced masks defining large contiguous zones of equal

emissivity, which are then subsequently subdivided in order to achieve the selected signal-to-noise ratio using the Voronoi tessellation. Previous applications of this technique is given by Simionescu et al. (2007) and is somewhat similar to the contour binning technique of Sanders et al. (2006).

3. MAPS

Using the constraints imposed by strong variations in the X-ray surface brightness, we have designed a mask of 130 regions which depict all the important details of M84. This mask optimally splits large regions into smaller ones using the Voronoi tessellation method. This method has been previously applied to XMM-*Newton* observations of M87 (Simionescu et al. 2007) and A3128 (Werner et al. 2007). This is a first application of this method to *Chandra* data. We published the results of this analysis using the meta-table format developed within the German Astrophysical Virtual Observatory (GAVO) and published as a web-service accessible at <http://www.g-vo.org/MAXI> and having a data release unique identifier (druid) of <http://www.g-vo.org/MAXI/druid/2>. This service allows one to view the parameters of the fit, access the quality of the fit, build, view and retrieve any maps and access the significance of every feature.

In the spectral analysis, we used the APEC model. In addition to the soft emission of M84, we clearly detect harder emission, which on smaller scales is centered on M84 and has been discussed in Finoguenov & Jones (2001), while on large scales is associated with emission of the Virgo cluster in which M84 is embedded. Thus, we introduced a second APEC model with temperature fixed at 3 keV and a fixed metallicity of 0.3 solar. Having two thermal models substantially reduces our ability to derive the metallicity in M84. Therefore, we have also fixed the metallicity of the APEC component describing the M84 emission to 0.3 solar, which is typical of the regions of M84 with bright X-ray emission.

Since the bubbles are symmetric about their center, but not with respect to the center of X-ray emission in M84, we have adopted a complex procedure for deriving the volumes, which require an estimate of the projected length. All bubble-related features are calculated assuming spherical symmetry relative to bubble centers, reported in Table 1. Other features are calculated using spherical symmetry relative to the center of X-ray brightness of M84. The exact details of our volume calculation and selecting the centers of the elements are presented in Mahdavi et al. (2005).

In order to study the fluctuations in the pressure and entropy, first we have analyzed the mean trends, following the procedure outlined in Sanderson et al. (2005), which puts the values of the map on the profile according to the distance to the center of the region, generates a non-parametric fit to the profile (using *R*-package) and calculates the residuals. Each region is treated as one point on the profile. Within this procedure the small differences in defining the center of the region (as e.g. discussed in Mahdavi et al. 2005) would result in differences in the mean profile but not in the ratios. In Figure 3 we show the ratio of the observed pressure to the mean pressure profile (left panel) and the analogous quantity for the gas entropy. The fractional rms fluctuations of en-

tropy and pressure caused by the AGN are on the level of 47% and 41%, respectively, with 5% measurement uncertainty. For comparison, in clusters of galaxies similar levels of fluctuations are associated with distortions due to a recent merger (Poole et al. 2007) and has about 10% occurrence probability at low redshift (Finoguenov et al. 2005, 2007). However, the features associated with cluster mergers appear on much larger spatial scales.

4. HYDRODYNAMICAL SIMULATIONS

In order to gain insights into the bubble physics, we embarked on hydrodynamical simulations. The details of the simulation used here can be found in Brügggen, Ruszkowski & Hallman (2005). Here we only summarize the relevant information. The initial conditions for the simulation were taken from the S2 cluster run (Springel et al. 2001) performed with the *GADGET* code. Starting from these initial conditions (at $z = 0$) we evolved the system for 140 Myr using the adaptive mesh refinement *FLASH* code. The full size of the computational domain was $2h^{-1}$ Mpc and the maximum resolution was $1.96h^{-1}$ kpc. While the cluster atmosphere and ICM parameters differ from those in M84, the initial conditions possess some characteristics that make the simulated system are qualitatively similar to M84. In particular, the structure is quite dynamic, the central object moves relative to the surrounding gas and the temperature in the central parts raises with radius as in M84.

5. WAVES

The main result from the maps in Fig.3 is the identification of the bubble walls with the regions of enhanced pressure (by a factor of 1.5) and simultaneously 40% lower entropy. Previously, the presence of shock waves has been often dismissed on grounds of low temperature contrast seen between the bubbles and the surrounding medium. Such comparison assumed a similarity in the entropy between the bubble walls and the surrounding medium. This is in contradiction to the observed entropy distribution seen in Figure 3, which shows that the gas associated with the bubble walls has low entropy. One would expect higher temperature in the compressed gas, if it were not for the fact that low temperature gas is entrained and moved to larger distances from the center thus partially cancelling the effect of adiabatic heating. Thus low temperature contrast may well be consistent with the wave scenario. We estimated that, on the time-scale of the bubble expansion (10^7 yr), the cooling (time scale of 10^9 yr) is not important and the origin of low entropy gas is due to entrainment from the central regions of M84. The entropy profile in M84 is rather steep and small gas displacements (compared to the bubble size) are sufficient to reproduce an observed picture.

We thus interpret the overpressured shells seen in M84 as waves propagating away from the sites where the energy has been injected by the AGN. The compression of the gas immediately outside the cavity is released in the form of a weak shock wave. Similar interpretation has also been presented in case of Perseus cluster (Fabian et al. 2003) and M87 (Forman et al. 2007). This interpretation is supported by the results of numerical simulations (see Fig.4). We also note that the observed fractional pressure fluctuations in the “walls” are larger than the fractional density fluctuations, which

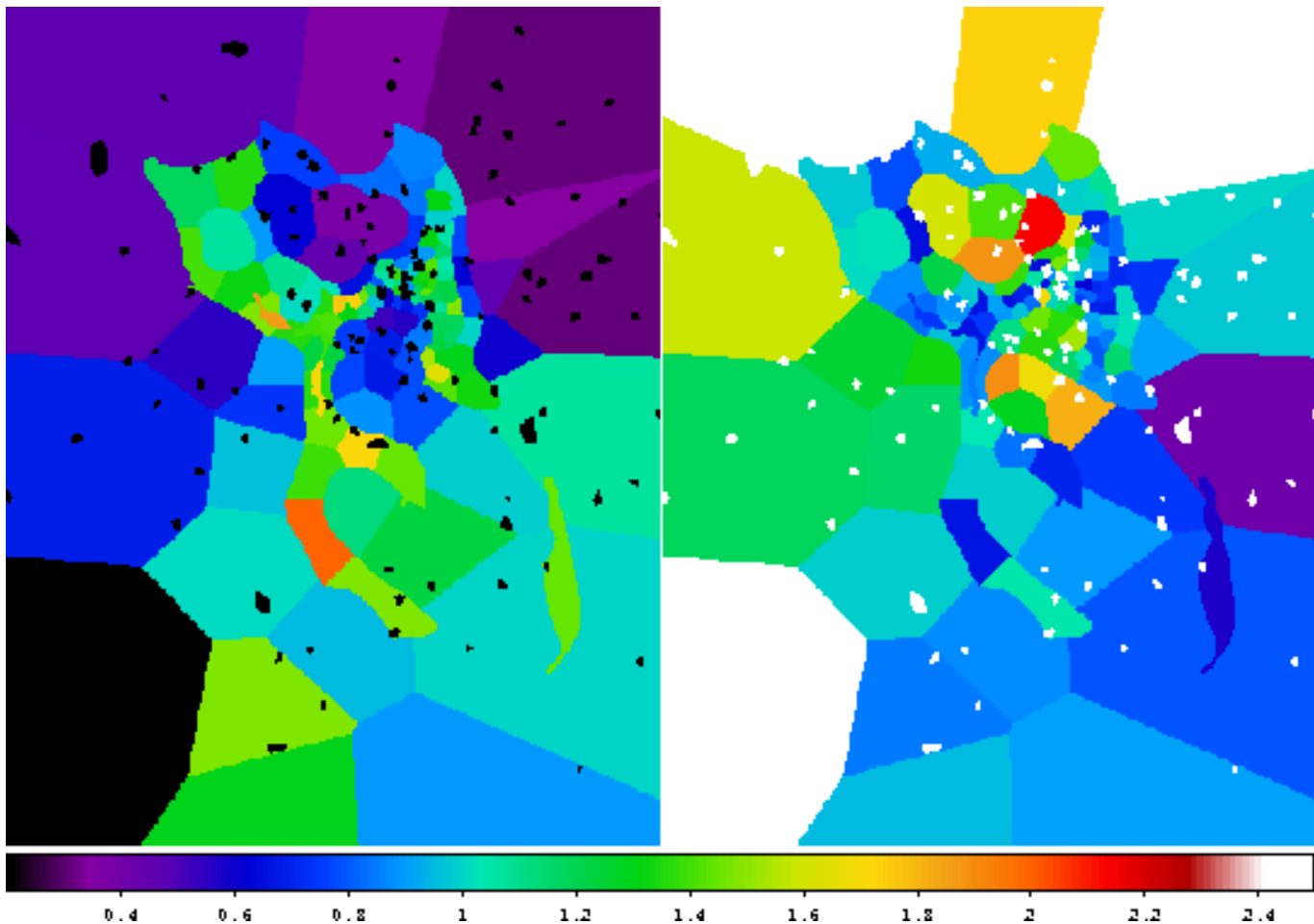


FIG. 3.— Ratio of the observed pressure *left* and entropy *right* in M84 to their corresponding average profiles. The values vary between 0.5 and 2. One can identify the bubble walls with a factor of 1.5 higher pressure and 40% lower entropy. Each image is 2.8×3.8 arcminutes (14×19 kpc) in size.

TABLE 1
CHARACTERISTICS OF BUBBLES IN M84

Bubble name	position of the center RA, Dec. (Eq. 2000)	axes kpc	λ/r	$(\lambda/r) \times (r/R)^3$	M	PV work 10^{55} ergs	wave energy 10^{55} ergs
Southern Large	186.26217 +12.869655	2.6 2.2 2.2	1/7	0.2	1.3	1.32	0.67
Southern Small	186.26680 +12.882228	1.4 1.5 1.4	1/4	0.6	1.3	0.30	0.37
Northern Small	186.26876 +12.890701	1.3 1.5 1.5	1/4	0.6	1.3	0.26	0.35
Northern Large	186.27185 +12.892204	2.0 2.9 2.9	1/7	0.2	1.3	1.37	0.72

is consistent with the adiabatic compression scenario. As a proof of concept, in Figure 4 we show a density slice corresponding to a snapshot from an adaptive mesh refinement hydro simulation of AGN feedback. The images have been unsharp-masked and Gaussian-blurred to enhance the fluctuations. There is a qualitative similarity between this figure and the morphology of M84. This figure shows that multiple outbursts can lead to nested waves similar to a Russian matryoshka doll. The upper panel corresponds to an earlier epoch and the snapshots are separated by approximately 2×10^7 years. The waves detach from the AGN-inflated cavities as is clearly seen in the lower panel. The northern cavity is further distorted due to the relative motion between the AGN and the ICM. Interestingly, the

evolution of the (nearly) vertical boundary between the northern bubbles seen in the simulation, shows that this feature is also a propagating wave (this is clearly seen in the animated version of the data). A similar feature is located "inside" the northern cavity in M84.

6. ESTIMATING AGN WORK

We estimate the energy carried in the waves using the following approach. The instantaneous energy flux F carried by a wave is given by:

$$F \equiv \frac{P_{\text{wave}}}{S} = \frac{(\delta P)^2}{\rho v_{\text{wave}}}, \quad (1)$$

where v_{wave} is the wave propagation velocity, P_{wave} is

the wave power, $S = 4\pi r^2$ where r is the distance of the wavefront from the bubble center, ρ is the ICM density and δP is the pressure fluctuation in the wavefront (Landau & Lifshitz 1987, Ruszkowski, Brügggen, & Begelman 2004, Sanders & Fabian 2007). Strictly speaking, Equation 1 is valid only for small perturbations, but it should suffice for our estimates as the inferred Mach number of the waves only slightly exceeds unity (see below). We assume that at any given time the wave front is a sphere, the instantaneous power of the entire wave is: $P_{\text{wave}} = 4\pi r^2 F$ [erg s⁻¹]. In the absence of dissipation, this (total) power would remain constant even though r , ρ , v_{wave} and δP would all vary. The total energy carried by one wave is then $E_{\text{wave}} \sim P_{\text{wave}} \lambda / v_{\text{wave}}$, where λ is the wavelength (or \sim the thickness of the pressure fluctuation). Approximating v_{wave} as the adiabatic sound speed, the final expression for the wave energy is:

$$E_{\text{wave}} \sim 3 \left(\frac{\lambda}{r} \right) \gamma^{-1} P V \left(\frac{\delta P}{P} \right)^2 \left(\frac{r}{R} \right)^3, \quad (2)$$

where V is the bubble volume, P is an underlying pressure, R is the bubble radius, r is the distance of the wavefront from the bubble center and γ is the adiabatic index of the gas in the vicinity of the wave. The pressure morphology of the source suggests that the ratio of the wave thicknesses to the radii of the wavefronts is approximately in the range $\sim 1/7$ to $1/4$ depending on the bubble position (e.g., $\sim 1/4$ for the small bubbles, $\sim 1/7$ for the large bubbles). If $r \sim R$, and using our observation of $\delta P/P \sim 1$, this would suggest that E_{wave} is of the order of PV . Even if the bubble energy is greater than PV by a few, one wave carries a significant fraction of the outburst energy. The result of this analysis is shown in Table 1, where wave energy is compared to PV work. The energy carried by the waves can significantly contribute to the overall energy budget. Note also that the smaller inner outbursts have larger wave-to-bubble energy ratios.

In addition to energy carried by the wave, we can calculate the energy deposition into the IGM associated with supersonic wave motion,

$$dQ = T dS = \frac{1}{\gamma - 1} \left(\frac{kT}{\mu m_p} \right) \frac{dS_x}{S_x}. \quad (3)$$

where $S_x = kT\rho^{1-\gamma}$ is a common definition of the entropy among X-ray observers. For the value of Mach number of 1.3 measured for M84 bubbles, and employing the Rankine-Hugoniot adiabat shock adiabat to derive the change in the entropy

$$1 + \frac{dS_x}{S_x} = \frac{(2\gamma M^2 - (\gamma - 1))((\gamma - 1)M^2 + 2)^\gamma}{(\gamma + 1)^{\gamma+1} M^{2\gamma}} \quad (4)$$

$\frac{dS_x}{S_x} = 0.013$ and the full energy deposition $dQdM_{\text{gas}}$ is a few percent of the total wave energy. The maximum deposition of energy occurs near the center of M84 and in the direction perpendicular to the bubble outflow, where also the cooling losses are largest. This probably results from interference of waves coming from northern and southern bubbles and is an important channel of energy deposition into the central parts of M84 IGM.

We note that using

$$\frac{dS_x}{S_x} = \frac{dP}{P} - \gamma \frac{d\rho}{\rho} \quad (5)$$

$dQdM_{\text{gas}}$ can be rewritten as

$$dQdM_{\text{gas}} = \int \frac{dP}{\gamma - 1} dV - \int \frac{\gamma}{\gamma - 1} P \frac{d\rho}{\rho} dV \quad (6)$$

The second part of the equation is negligible in the case of strong shock ($M > 1000$) which leads to the equation used by Graham et al. (2008). We note, however, that in our case the two terms are nearly equal and in case of adiabatic compression they exactly cancel out. The total heating supplied by AGN, when compared to 9.4×10^{40} bolometric luminosity associated with *extended* emission of M84 (not counting the contributions from AGN and LMXB), requires a bubble recurrence on the 1.8×10^7 yr scale to entirely compensate for the radiative energy losses, similar to what is actually observed in M84.

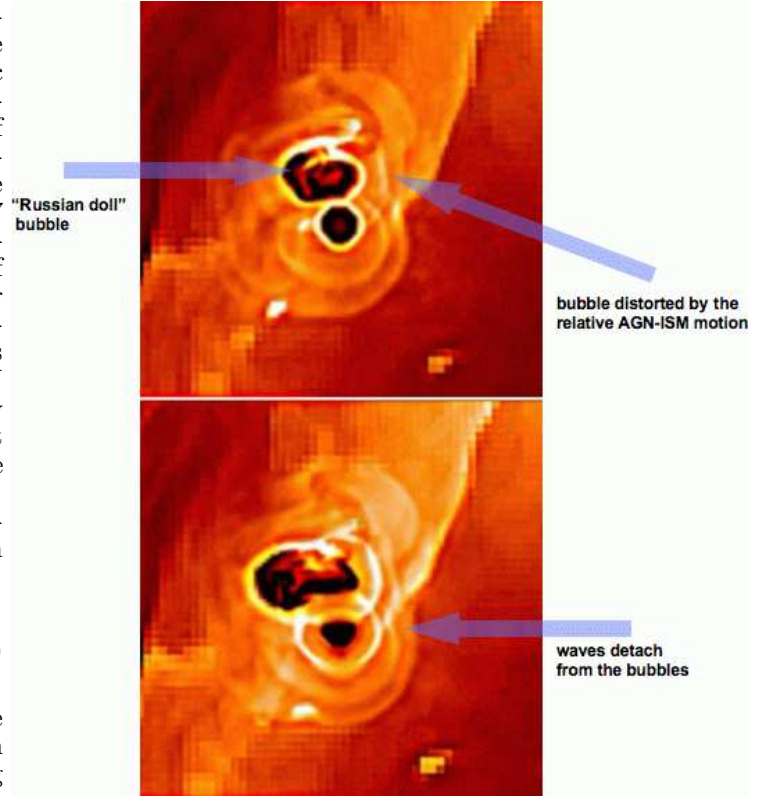


FIG. 4.— Subsequent density snapshots from an adaptive mesh simulation of AGN feedback in a galaxy cluster. The box sizes in both panels are about $300^{-1}h$ kpc on a side. See text for details.

The morphology of the southern shells seen in the data suggests that the expansion velocity is comparable to the velocity of M84 relative to the ICM. A typical velocity of a cluster galaxy is expected to be mildly supersonic (Faltenbacher et al. 2006). This is because $c_s^2 = \gamma P_{\text{gas}} / \rho = \gamma \sigma_{\text{gas,1D}}^2 = \gamma \sigma_{\text{gas,3D}}^2 / 3 = \gamma \sigma_{\text{gal}}^2 / 3$, where $\sigma_{\text{gas,1D}}$ and $\sigma_{\text{gas,3D}}$ are the one-dimensional and three-dimensional gas internal velocity dispersions, respectively, and σ_{gal} is the galaxy velocity dispersion (Sarazin 1988). The last approximate equality comes from the assumption of equipartition between the gas and the galaxies. For

$\gamma = 5/3$ this leads to the galaxy Mach number ~ 1.34 . This in turn suggests that the shell expansion may be, at least initially, supersonic. If so, this would also be consistent with an estimate of the Mach number of the waves. If the pressure fluctuation is $x = \delta P/P \sim 1$ as suggested by our observations, then for $\gamma = 5/3$, the Mach number of the waves is $M \sim [(1 + \gamma^{-1})x/2 + 1]^{1/2} \sim 1.34$ in qualitative agreement with the estimate above.

7. CONCLUSIONS

We have analyzed a deep *Chandra* observation of the AGN feedback in the Virgo elliptical galaxy M84. We have applied a constrained Voronoi tessellation binning method to *Chandra* data. Our main results are: (1) the AGN outflow is mildly supersonic, (2) the non-thermal plasma from the AGN-inflated cavities appears to be porous and the non-thermal particles escape from the cavities, (3) co-centric density perturbations (weak shock waves) are present and their morphology is qualitatively consistent with the results of numerical simulations, (4)

we have estimated the mechanical energy in the waves and found that it may contribute substantially to the overall mechanical energy delivered by the AGN.

AF acknowledges support from BMBF/DLR under grant 50 OR 0507. AF thanks CfA for hospitality during his visits. AF thanks Jaiwon Kim and Gerard Lemson for their help in publishing the data through GAVO. MR acknowledges *Chandra* Theory grant TM8-9011X. MB acknowledges the support by the DFG grant BR 2026/3 and the supercomputing grants NIC 2195 and 2256 at the John Neumann Institut (NIC) in Julich. The results presented were produced using the *FLASH* code, a product of the DOE ASC/Alliances-funded Center for Astrophysical Thermonuclear Flashes at the University of Chicago. The authors thank the anonymous referee for insightful report, that helped to improve the material presented in this paper.

REFERENCES

- Binney, J., Bibi, F. A., & Omma, H. 2007, MNRAS, 377, 142
 Brügggen, M., Ruszkowski, M., & Hallman, E. 2005, ApJ, 630, 740
 Cappellari, M., & Copin, Y. 2003, MNRAS, 342, 345
 Diehl, S., Li, H., Fryer, C., & Rafferty, D. 2008, ArXiv e-prints, 801, arXiv:0801.1825
 Fabian, A. C., Sanders, J. S., Allen, S. W., Crawford, C. S., Iwasawa, K., Johnstone, R. M., Schmidt, R. W., & Taylor, G. B. 2003, MNRAS, 344, L43
 Faltenbacher, A., & Diemand, J. 2006, MNRAS, 369, 1698
 Finoguenov, A., & Jones, C. 2002, ApJ, 574, 754
 Finoguenov, A., & Jones, C. 2001, ApJ, 547, L107
 Finoguenov, A., Böhringer, H., & Zhang, Y.-Y. 2005, A&A, 442, 827
 Finoguenov, A., Ponman, T. J., Osmond, J. P. F., & Zimer, M. 2007, MNRAS, 374, 737
 Finoguenov, A., Böhringer, H., & Zhang, Y.-Y. 2005, A&A, 442, 827
 Forman, W., et al. 2007, ApJ, 665, 1057
 Graham J., Fabian A. C., Sanders J. S., 2008, MNRAS, 386, 278
 Landau, L. D., & Lifshitz, E. M. 1997, Fluid Mechanics (Oxford: Pergamon)
 Mahdavi, A., Finoguenov, A., Böhringer, H., Geller, M. J., & Henry, J. P. 2005, ApJ, 622, 187
 Mazzotta, P., Kaastra, J. S., Paerels, F. B., Ferrigno, C., Colafrancesco, S., Mewe, R., & Forman, W. R. 2002, ApJ, 567, L37
 McNamara, B. R., & Nulsen, P. E. J. 2007, ARA&A, 45, 117
 Poole, G. B., Babul, A., McCarthy, I. G., Fardal, M. A., Bildfell, C. J., Quinn, T., & Mahdavi, A. 2007, MNRAS, 380, 437
 Ruszkowski, M., Brügggen, M., & Begelman, M. C. 2004, ApJ, 615, 675
 Sanders, J. S. 2006, MNRAS, 371, 829
 Sanders, J. S., & Fabian, A. C. 2007, MNRAS, 381, 1381
 Sanderson, A. J. R., Finoguenov, A., & Mohr, J. J. 2005, ApJ, 630, 191
 Sarazin, C.L., "X-ray Emission from Clusters of Galaxies," Cambridge: Cambridge University Press
 Simionescu, A., Böhringer, H., Brügggen, M., & Finoguenov, A. 2007, A&A, 465, 749
 Springel, V., et al. 2001, ApJ, 549, 681 (erratum 562, 1086)
 Vikhlinin, A., Markevitch, M., Murray, S. S., Jones, C., Forman, W., & Van Speybroeck, L. 2005, ApJ, 628, 655
 Werner, N., Churazov, E., Finoguenov, A., Markevitch, M., Burenin, R., Kaastra, J. S., Böhringer, H. 2007, A&A, 474, 707